Research Paper

Plasma-catalytic conversion of CO_2 and CO_2/H_2O in a surface-wave sustained microwave discharge

Guoxing Chen [a,b,*], Thomas Godfroid [c], Nikolay Britun [a], Violeta Georgieva [b], Marie-Paule Delplancke-Ogletree [b], Rony Snyders [a,c]

[a] ChIPS, Université de Mons, 23 Place du Parc, 7000 Mons, Belgium
[b] 4MAT, Université libre de Bruxelles, 50 av. F.D. Roosevelt, 1050 Brussels, Belgium
[c] Materia Nova Research Center, av. N. Copernic 1, 7000 Mons, Belgium

ABSTRACT

The conversion of CO_2 and CO_2/H_2O mixtures on a TiO_2 supported NiO catalyst in a pulsed surface-wave sustained microwave discharge has been investigated. The influence of the catalyst preparation method (conventional calcination (in air or Ar) vs. Ar plasma-assisted decomposition) on the CO_2 conversion and its energy efficiency has been studied. The results demonstrate that the Ar plasma-treated catalyst is more active compared to the conventional calcined one. The plasma-treated catalyst increases the CO_2 conversion and its energy efficiency almost by a factor of two, compared to the plasma only assisted CO_2 dissociation, while the conventional calcined catalysts affect the CO_2 conversion rather insignificantly. The conversion of CO_2 is found to be about 45% at 70 Torr in pure CO_2 with Ar plasma-treated catalyst, having an energy efficiency of 56%. In the case of CO_2/H_2O mixture, the CO_2 conversion efficiency reaches 42% (energy efficiency is 52%) at 60 Torr. The catalyst characterization shows that Ar plasma treatment may result in a higher density of oxygen vacancies and a comparatively uniform distribution of NiO on the TiO_2 surface. The dissociative electron attachment of CO_2 at the catalyst surface enhanced by the oxygen vacancies and plasma electrons may explain the increase of conversion and energy efficiencies in this case. A mechanism of plasma–catalytic conversion of CO_2 at the catalyst surface in CO_2/H_2O mixture is proposed.

© 2017 Elsevier B.V. All rights reserved.

1. Introduction

The depletion of fossil fuel reserves and massive CO_2 emission during their combustion, have emphasized the issue of energy sustainability and environmental protection. Carbon capture and utilization (CCU) is one of the most promising solutions to limit the amount of greenhouse pollutions to the atmosphere. The idea of CCU is to capture and convert CO_2 into a carbon compound used as materials or energy carriers. In this case, CCU intends to slow down the rate of emissions via recycling of CO_2 which would otherwise be emitted in the atmosphere. A promising solution is the use of CO_2-free electrical energy produced, for example, by renewable or nuclear sources for dissociation of CO_2 or other greenhouse gases, followed by their conversion into easily storable synthetic fuels. In this context, the CO_2 re-utilization to synthesize syngas, fuels or chemical compounds as well as pure CO_2 dissociation into CO and O_2, is of a special interest.

Non-thermal plasmas provide an attractive alternative to the conventional catalytic pathway for greenhouse gas conversion [1], mainly due to their non-equilibrium properties and low power requirements which allow to sustain both physical and chemical reactions at relatively low gas temperatures [1]. Recently, the combination of heterogeneous catalysis and plasma, known as plasma-catalysis, has attracted tremendous interest for gaseous pollutant abatement [2,3], greenhouse gas reforming [4–6] and catalyst treatment [7–9]. The integration of plasma and solid catalysts has great potential to generate a synergistic effect, reducing the activation barrier of different reactions and improving the conversion rates, as well as the energy efficiency of the plasma process. In the past decade, non-thermal plasmas have been shown to be effective and efficient for activation of CO_2 [1,8,10–30]. Plasma-assisted dissociation of CO_2 has been explored using different non-thermal plasma sources. However, most previous works have mainly focused on the conversion of CO_2 diluted with noble gases (such as He and Ar) under very low flow rates, which less attractive for the industrial scale applications [14,16,17].

* Corresponding author at: Université de Mons, 23 Place du Parc, 7000 Mons, Belgium/Université libre de Bruxelles, 50 av. F.D. Roosevelt - CP165/63, 1050 Brussels, Belgium.
E-mail address: guoxchen@ulb.ac.be (G. Chen).

To synthesize a fuel, CO_2 is often combined with hydrogen-containing gases such as H_2 [31–33], CH_4 [4–6], or H_2O [34–36]. Since water is a promising source of hydrogen due to its abundance and low cost, there is a big interest to investigate plasma assisted H_2O-CO_2 conversion as an alternative system for conversion of CO_2 to value-added chemicals. Up to now, only few studies have investigated the non-thermal plasma- driven catalysis for conversion of CO_2 in the presence (or absence) of H_2O [8,10,35]. Further fundamental work is still required to optimize and improve the mentioned plasma-based and water-assisted conversion process. In addition, finding a correct and cost-effective catalyst to achieve high energy efficiency and a high conversion rate is a great challenge as very few research works have been focused on plasma-catalytic CO_2 conversion [8,14,19,20].

Plasma is being increasingly used as a tool for preparing catalysts for conventional thermal processes [7–9,37–40]. The non-thermal plasma, having highly energetic electrons and chemically reactive species (e.g. free radicals, excited atoms, ions, and molecules), can modify surface properties of the catalyst, enhance the dispersion of the supported metals, and even create a disorder in their crystallite structure, depending on the nature of the gas phase and experimental treatments conditions. Indeed, by using cold plasma, many highly active and durable catalysts have been prepared for CO_2 and methane conversion as well as for NO_x abatement [7–9]. In both cases, catalyst and plasma combined reactions, it is expected that plasma would modify the physico-chemical properties of a catalyst in situ, after which the modified catalyst would demonstrate high performance in the plasma reaction [1].

The advantages of microwave plasma combined with Ar plasma-treated catalyst for greenhouse gas dissociation were discussed in our previous work, where the decomposition of CO_2 and a mechanism of plasma-catalysis synergy on the catalyst surface were proposed [8]. The goal of the present work is to study the relationship between the catalyst preparation method and the catalyst surface modifications in terms of structure, morphology and defect formation, and finally determine the effect of these modifications on the decomposition of CO_2 in different gas mixtures. To achieve this goal, we used a non-equilibrium microwave discharge combined with TiO_2 supported NiO catalysts. The influence of two different catalyst preparation methods (conventional calcination vs. Ar plasma treatment) on the CO_2 conversion and the energy efficiencies is studied. The synergistic effect obtained by combining plasma and catalyst for the decomposition of pure CO_2 or CO_2 mixed with H_2O or H_2 has been investigated from both physical and chemical perspectives through the correlation of catalyst characterization with the plasma catalysis activity data.

2. Experimental

2.1. The microwave discharge reactor

The experimental setup for pulsed microwave plasma generation used in this work is shown schematically in Fig. 1. The discharge is generated at 0.915 GHz in a quartz tube with a 14 mm inner diameter and 31 cm length, cooled by 5 °C oil flowing between the inner and the outer (polycarbonate) tubes. The whole system is surrounded by a grounded aluminum grid preventing leakage of microwave radiation into the outer space. The impedance of the waveguide has been adapted by an automatic three stubs system in order to minimize the reflected microwave power. The reflected power in most cases was below the detection limit and thus considered negligible. The CO_2 or the other gases (Ar, H_2 or H_2O) used in the present study are injected from the top of the system with a flow rate regulated by electronic mass flow controllers ranging between 0 and 6 standard liter per minute (slm). The water vapor is generated in a commercial (Omicron) vaporization system. The water vapor flow rate varies between 0 and 1 slm. A chamber containing the catalyst is connected to the end of the plasma tube so that the catalyst is positioned at around 2 cm below the quartz tube end. A thermocouple is installed inside the catalyst chamber in order to measure the gas temperature in the post discharge. In each experiment 8 g of catalysts were used. The pressure in the discharge has been controlled by changing the gas pumping speed by a throttle valve. Pulsed plasmas with pulse duration of 300 μs, and a period of 600 μs were used. A more detailed description of the microwave set-up can be found in [24,41].

2.2. Analysis of the decomposition products

The gas composition in the post-discharge region has been analyzed by a Bruker 450-GC gas chromatograph (GC) equipped with a carbon molecular sieve column and a molecular sieve 5A column in series and connected to a thermal conductivity detector. Argon was used as a carrier gas. The following main products were detected: CO_2, CO, H_2 and O_2. In this study, no carbon deposition has been observed after the plasma conversion of CO_2 with or without a catalyst. A very weak peak corresponding to formic acid was detected by GC in the CO_2-H_2O and CO_2-H_2 mixture cases. Nevertheless, the signal remains too weak to allow for a quantitative analysis. As the discharge worked at reduced pressure, a sampling system was used between the post-discharge and the gas chromatograph (Fig. 1). The low pressure sample is diluted with neutral gas until a pressure of 1.5 bar is reached, prior to its injection in the chromatograph. The microwave discharge has been also characterized by optical emission spectroscopy (OES). An Andor Shamrock-750 monochromator and an iStarDH740-18F-03 Intensified charge coupled device (ICCD) camera were used for spectral acquisition. The plasma emission was guided to the spectrometer by a visible-to-near infrared (VIS–NIR) optical fiber with a collimating lens. Several discharge parameters (such as gas temperature and vibrational temperature) were investigated in this paper based on the OES analysis, as described below.

2.3. Catalyst preparation

10 wt.% of NiO supported on TiO_2 catalysts were prepared by a combination of impregnation and plasma treatment methods. The precursor was Ni nitrate hexahydrate $Ni(NO_3)_2 \cdot 6H_2O$ (Merck). Pure anatase TiO_2 monocrystalline powder (Sigma-Aldrich) was used as a catalyst support. TiO_2 support was impregnated with the aqueous solution of $Ni(NO_3)_2 \cdot 6H_2O$ for 24 h and dried at 100 °C in air for 12 h. After impregnation and drying, the samples were prepared by the conventional method (thermal calcination) and by plasma treatment. In the conventional calcination process, the samples were calcined either in air or in Ar for 2 h at 300 °C. The two catalysts are denoted in the text as NiO/TiO_2(Air-C) and NiO/TiO_2(Ar-C). In the plasma treatment, the sample was treated by an Ar plasma during 2 h at a constant temperature (300 °C). The catalyst is denoted as NiO/TiO_2(Ar-P).

2.4. Catalyst characterization

The surface area of the catalyst was determined by nitrogen adsorption at 77 K with Brunauer-Emmett-Teller (BET) analysis.

Analysis of the crystalline structure of the catalyst was conducted by X-ray diffraction (XRD) in a Bruker advanced X-ray diffractometer (40 kV, 40 mA) using a Cu Kα (0.154 nm) at a scanning rate of 2 °/min from 20° to 90°.

Surface morphology of the samples has been examined by SU-70 Hitachi scanning electron microscope (SEM). The sample surface
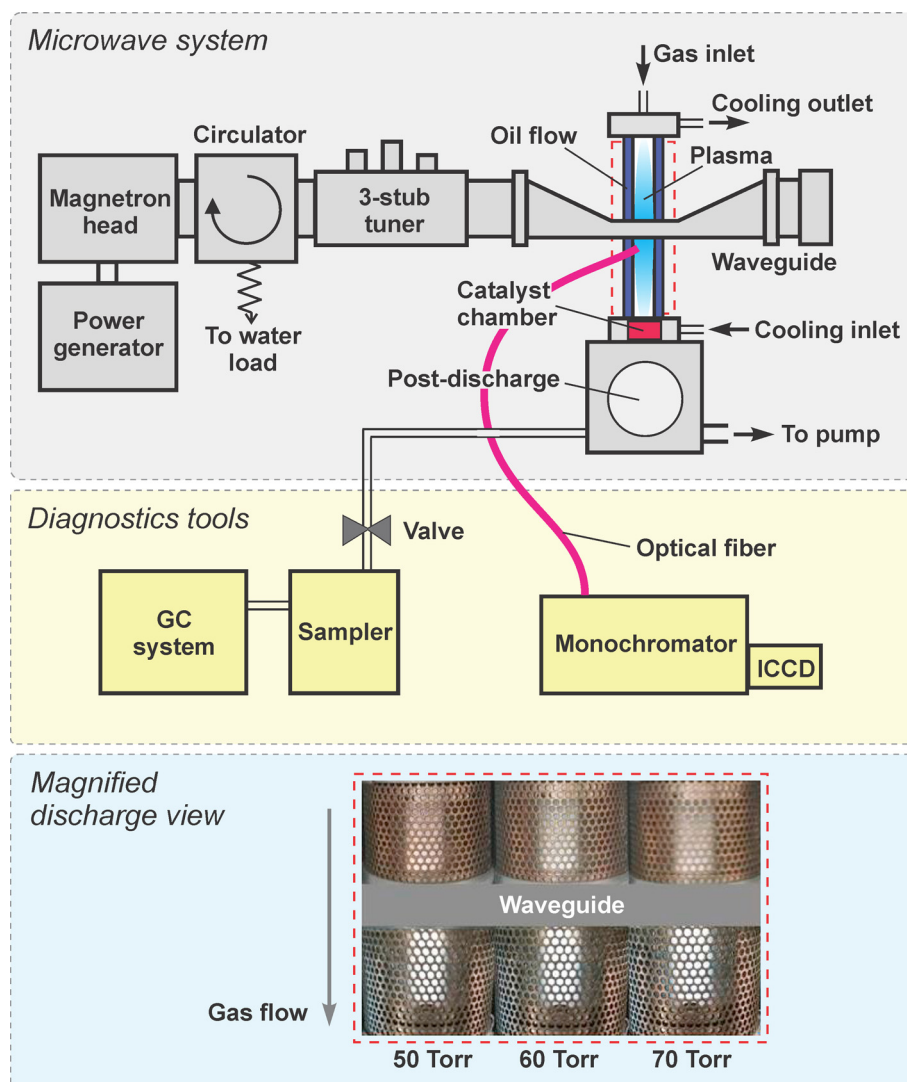
Fig. 1. Schematic representation of surface-wave microwave system, the diagnostics tool used, and the magnified discharge view.

and cross section were coated with gold by sputtering prior to introduction into the SEM chamber.

The sizes and morphology were obtained by transmission electron microscopy (TEM) imaging (Philips CM 200). For the TEM measurements, the catalyst samples were prepared by ultra-sonication in ethanol, followed by drop casting of the resultant suspension onto a carbon-coated copper grid.

The Raman spectra of the catalysts were recorded using a Raman spectrometer (Bruker) under ambient conditions, using a 532 nm argon ion laser as the excitation source. The spectral resolution was $0.5\,cm^{-1}$ and laser power was 2 mW. The Raman spectrometry was used to detect defects in the crystal lattice.

X-ray photoelectron spectroscopic (XPS) measurements were performed using a ESCA-5000 (Physical Electronics) Versa Probe system. The XPS data were collected using monochromatic Al Kα radiation at 1486.6 eV. All XPS spectra were referenced to the C1 s peak at 285 eV in order to compensate the charge effect.

3. Results and discussion

3.1. Phase structure and morphology

The X-ray powder diffraction patterns of the conventional calcined and plasma-treated catalysts are presented in Fig. 2.
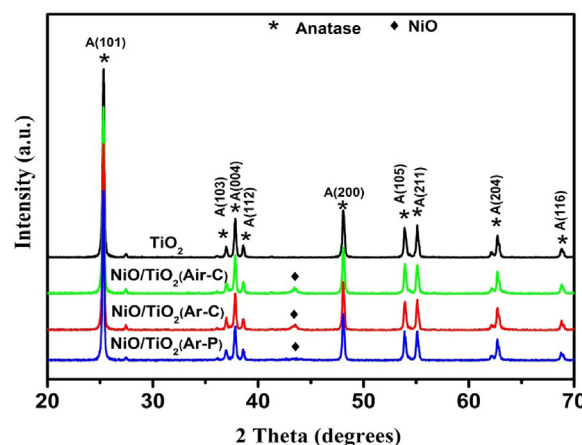

Fig. 2. XRD patterns of the conventional calcined and plasma-treated catalysts and pure TiO_2.

Regardless of the preparation method, the anatase phase of TiO_2 is observed. In addition, a diffraction peak at $2\theta = 43.5°$ corresponding to the (200) crystal planes of face-centered cubic NiO appears on the XRD patterns of the NiO/TiO_2 catalysts (both conventional calcined
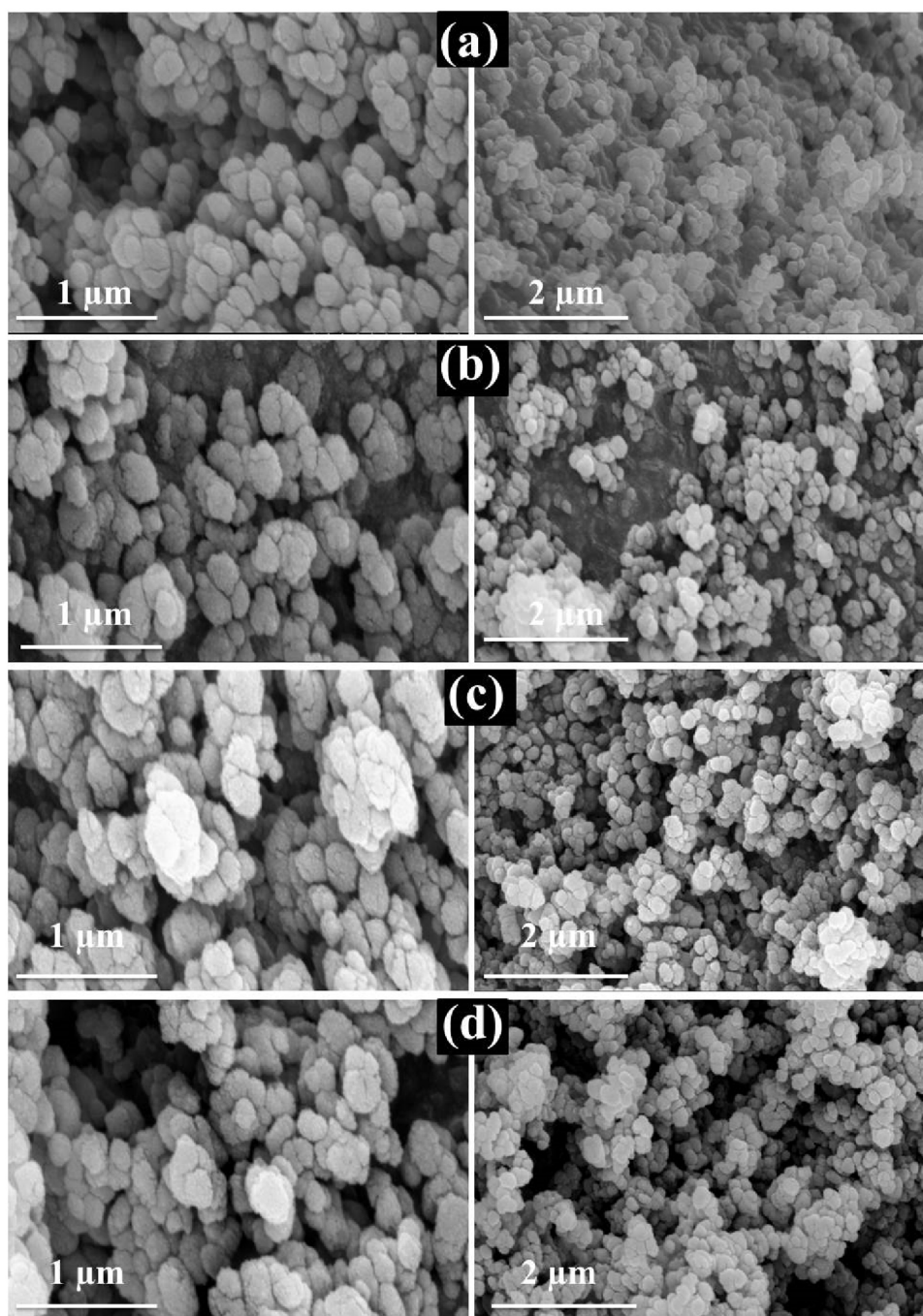
Fig. 3. SEM micrographs of (a) TiO_2, (b) $NiO/TiO_2(Air-C)$, (c) $NiO/TiO_2(Ar-C)$ and (d) $NiO/TiO_2(Ar-P)$.

and plasma treated). Table S1 gives the lattice parameters (lattice constants a and c), the crystallite size (calculated using Scherrer's equation on (101) diffraction peak) and the BET surface area for the catalysts and pure TiO_2 support. Similar crystallite sizes ($\sim$46 nm) were observed for all samples. The largest increase (constant c) is observed for the $NiO/TiO_2(Ar-P)$ sample. This is explained by the substitution of Ti ions by larger Ni ions in the TiO_2 crystal lattice [8]. On the other hand, the same increase of the BET surface area was measured for all samples with the addition of NiO. This could be attributed to the dispersion of NiO particles on the surface of the TiO_2 nanoparticles consistently with the XRD observation.

In addition to the structural characterizations, SEM and TEM analyses were carried out to evaluate morphology of the conventional calcined and plasma-treated catalysts (Fig. 3 and Fig. 4). The

particle sizes and morphology of the catalysts prepared using the different methods appeared to be very similar, exhibiting oval-like grains (Fig. 3). Nevertheless, by using TEM, it is observed that for the $NiO/TiO_2(Ar-P)$ sample (Fig. 4(c)) the NiO particles are spread over the TiO_2 support with a better covering of the support in comparison with the thermally treated sample (Fig. 4). Spot analysis on the TEM-EDS (energy dispersive x-ray spectroscopy) confirmed that Ni^{2+} was dispersed on the surface of TiO_2 (See Fig. S1).

3.2. Raman spectral analysis

The Raman spectroscopy is used in order to confirm the XRD data and to identify the presence of defects in the catalysts and TiO_2 support. Five peaks located at about 638, 516, 397, 196, and
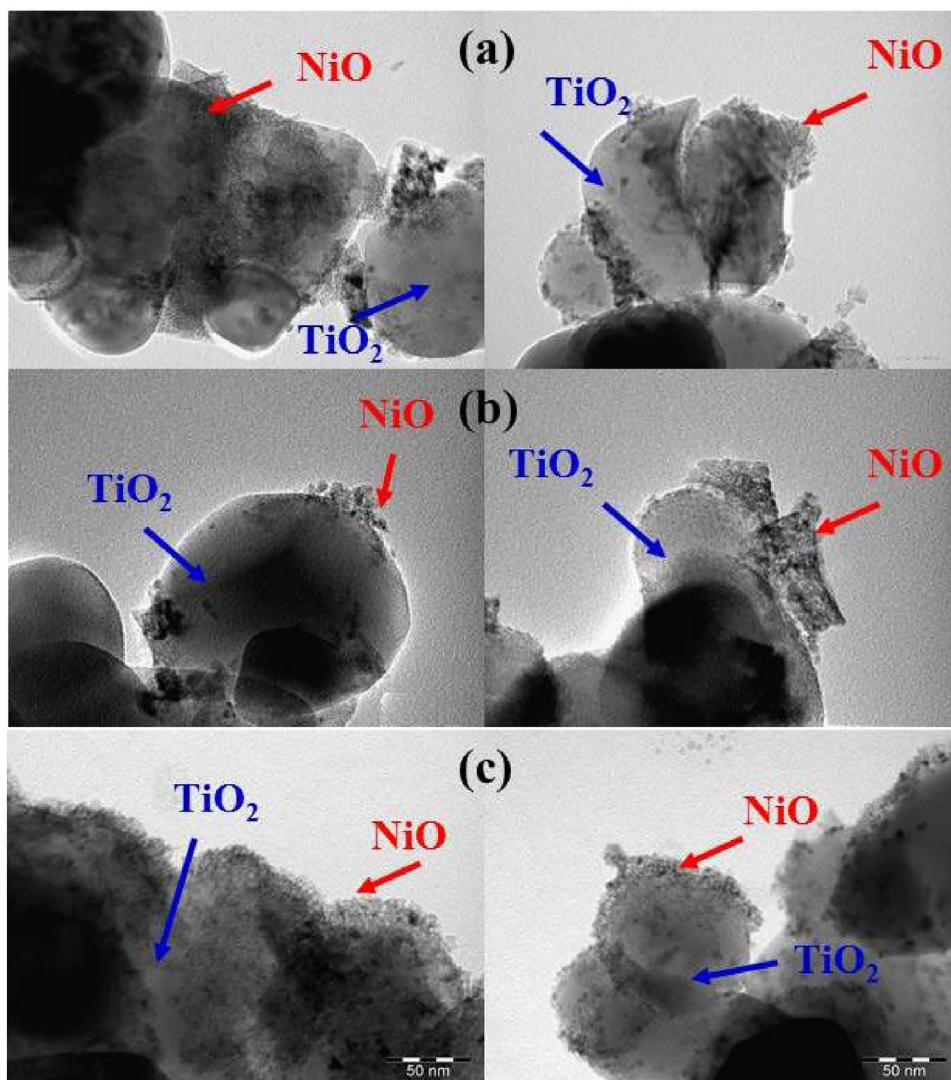
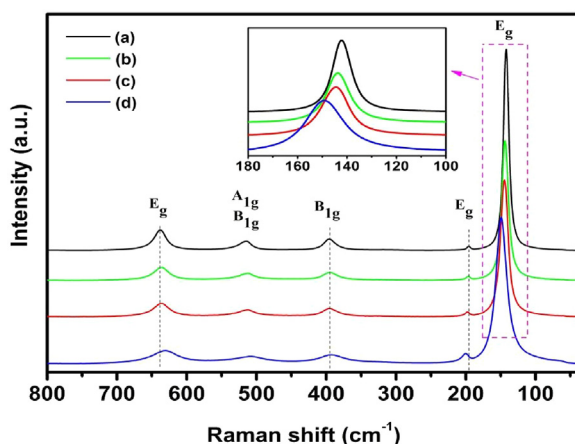**Fig. 4.** TEM micrographs of (a) NiO/TiO$_2$(Air-C), (b) NiO/TiO$_2$(Ar-C), and (c) NiO/TiO$_2$(Ar-P).

Fig. 5. Raman spectra of (a) TiO$_2$, (b) NiO/TiO$_2$(Air-C), (c) NiO/TiO$_2$(Ar-C) and (d) NiO/TiO$_2$(Ar-P).

Fig. 6. Full width at half-maximum (FWHM) in E$_g$ modes in the different catalysts and TiO$_2$ support.

142 cm^{-1} are observed in all samples (Fig. 5). These peaks are assigned to the E$_g$, (B$_{1g}$/A$_{1g}$), B$_{1g}$, E$_g$ and E$_g$ modes, respectively [42–44]. They correspond to the characteristic Raman modes of the anatase TiO$_2$ structure. Compared to the pure TiO$_2$, the 142 cm^{-1}
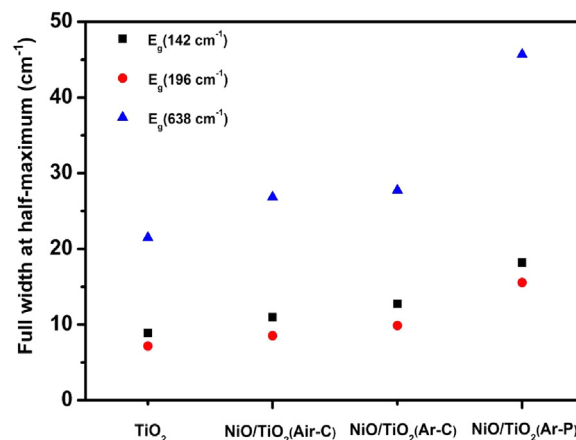
and 196 cm^{-1} peak present a blue shift for the NiO/TiO$_2$ catalyst while the 638 cm^{-1} peak is red shifted. Fig. 6 shows the full width at half-maximum (FWHM) of the E$_g$ modes measured for the different samples. It shows that the E$_g$ peaks of NiO/TiO$_2$ catalysts are

broadened relatively to pure TiO_2. These measurements show that the vibrations of the TiO_2 crystal lattice are considerably affected by the presence of Ni ions. Indeed, the E_g peaks are associated with the symmetric stretch vibration of O—Ti—O in TiO_2. This mode is very sensitive to local oxygen coordination surrounding the metal ion [45,46]. According to previous detailed analysis of Raman spectra of TiO_2 and doped-TiO_2 samples [8], the broadening and shifting of the main bands are caused by the presence of oxygen vacancies. As it is visible from Fig. 5 and Fig. 6, the largest shift and broadening occur for the Ar plasma treated (NiO/TiO_2 (Ar-P)) catalyst. These results indicate that the plasma-treatment of the catalyst results in a higher density of oxygen vacancies compared to the conventional calcined samples.

The pure TiO_2 support and the TiO_2 support pre-treated with Ar plasma were also investigated in our previous study [8]. No influence of Ar plasma pre-treatment was found on the crystalline structure and active surface area of TiO_2 support, as well as, on the defect formation. Therefore, an important condition for the formation of oxygen vacancies in Ar plasma pre-treated catalyst is the

presence of Ni or NiO. Our XRD and microcopy results suggest that Ar plasma treatment result in a very good distribution of Ni oxide on the TiO_2 surface offering the possibility for a more efficient Ni^{2+} doping of the TiO_2 lattice (also suggested by the c lattice parameters shift). These oxygen vacancies created by substituting Ni^{2+} on the Ti^{4+} sites are more stable than those obtained by the thermal treatment of stoichiometric TiO_2. It was shown that the oxygen vacancies in TiO_2, generated from thermal treatment with inert gas (He) under atmospheric pressure, were not stable in air [47].

3.3. XPS analysis

In order to perform an in-depth study of the chemical composition and oxidation states of the elements present on the catalyst surface, XPS measurements were carried out. Fig. 7 shows the high resolution XPS spectra of Ni 2p, O 1s and Ti 2p on the different NiO/TiO_2 samples. As shown in Fig. 7(a–c), it is clear that the XPS spectra of Ni 2p can roughly be divided into two edges, referred to as 2p 3/2 and 2p 1/2, respectively. The peaks at about 855.4 and
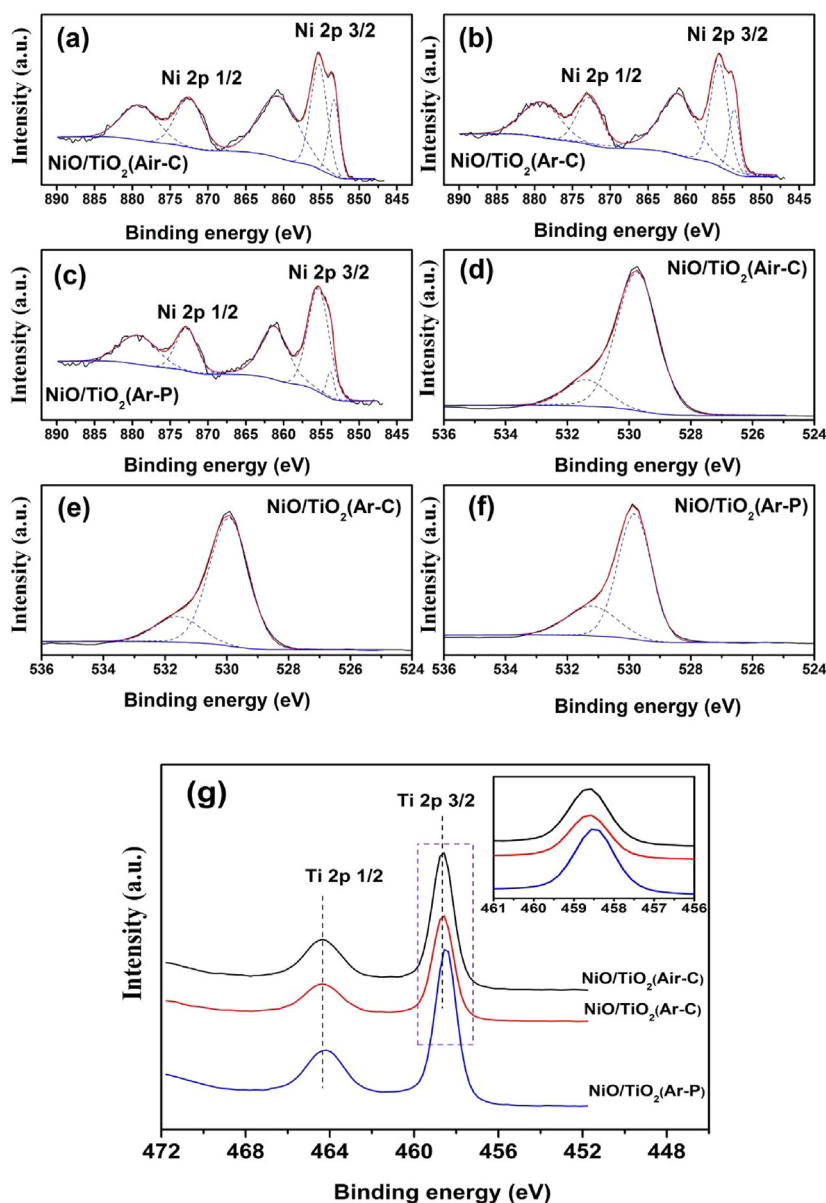

Fig. 7. XPS spectra of Ni 2p (a–c), O 1 s (d–f) and Ti 2p (g) on the different NiO/TiO_2 catalysts.

872.6 eV are Ni 2p 3/2 and Ni 2p 1/2, with the corresponding satellites peaks around 853.3, 860.8 and 879.2 eV. Similar results were also reported elsewhere [48–50]. All the peaks in Fig. 7(a–c) are assigned to Ni^{2+}. As shown in Fig. 7(d–f), the peak at about 529.7 eV can be assigned to lattice oxygen in the metal oxides, whereas the peak at about 531.4 eV can be ascribed to adsorbed oxygen or oxygen in the hydroxyl groups (adsorbed species H_2O, surface-OH) [51–53]. From the XPS spectra of Ti 2p (Fig. 7(g)), two broad peaks observed at 458.6 eV for Ti 2p 3/2 and 464.4 eV for Ti 2p 1/2. These peaks are corresponding to Ti^{4+} in TiO_2 [53–55]. The spectrum of NiO/TiO_2 (Ar-P) shows a slight shift compared to the spectrum of the other two samples. The Ti 2p 3/2 binding energy of NiO/TiO_2 (Ar-P) shifts about 0.2 eV toward low binding energy, compared to that of NiO/TiO_2(Air-C) and NiO/TiO_2(Ar-C). This shift indicated an influence of Ni addition on the electronic states of Ti element by the Ar plasma treatment. Probably some of the Ti^{4+} ions get substituted with Ni^{2+} ions in the lattices. This observation is consistent with the results published in the literature for TiO_2 doped with Fe or N [53,55].
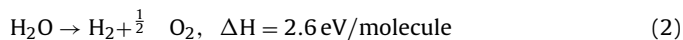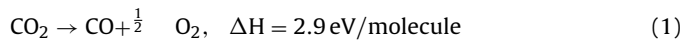
3.4. Plasma simulation

As discussed in the Section 3.1, Ar plasma treatment results in better dispersion of the supported metals on the TiO_2 surface. Molecular mechanisms of the reactions running with the participation of cold plasma, constituting a complex state containing highly active species, such as ions, electrons, radicals, and excited molecules, are generally entirely different from the "classic" chemical processes occurring during the conventional catalyst preparation [56]. However, the role of Ar plasma treatment on the catalyst modification remains rather hidden. In the current discharge geometry, experimental measurements are not always possible at different positions in the plasma tube or on the catalytic surface because of the solid metallic parts surrounding the setup in order to prevent microwave energy leakage (see Section 2). Therefore, computer modelling of the plasma and afterglow regions can bring a valuable insight in the catalyst activation process. In this study, we investigated it by a computational fluid dynamics approach using a 2-D model developed in the modelling platform PLASIMO [57,58]. It is based on solving self-consistently Maxwell's equations describing the electromagnetic field and the set of plasma fluid equations. The description of the model itself as well as its comparison with the experimental measurements is available elsewhere [59]. In our case the model is developed for Ar plasma taking into account the following species: electrons, Ar neutrals, atomic Ar^+ and molecular Ar_2^+ ions and two excited states grouping at the 4s and 4p levels each, Ar(4s) and Ar(4p). The electron density and energy distributions obtained at the operating conditions in continuous regime, close to the operating conditions for Ar plasma treatment of catalysts in pulsed regime, were already discussed in our previous study [8]. While the electron density and energy are important for the dissociative electron attachment of CO_2 on the catalytic surface, the impact of the heavy long-living particles from plasma may also supply energy to the catalyst surface, activate the surface diffusion and accelerate surface reactions. To clarify this point, the density profiles of the excited Ar(4s) and Ar(4p) states are presented in Fig. S2. The maximum values of Ar(4s) and Ar(4p) densities are found close to the tube wall and at the catalyst chamber region. As expected, the maximum density of the Ar(4s) states is higher (e.g. about 1 order of magnitude) than that of the Ar(4p) states, which is due to their metastable nature. This may imply effective catalyst activation by Ar metastables.

3.5. Plasma catalysis for conversion of CO_2 and CO_2/H_2O

3.5.1. Brief theoretical background

The dissociation of a CO_2 and H_2O molecules is represented by the following global reactions [10]:

$$CO_2 \rightarrow CO + \tfrac{1}{2} \quad O_2, \quad \Delta H = 2.9 \, eV/molecule \tag{1}$$

$$H_2O \rightarrow H_2 + \tfrac{1}{2} \quad O_2, \quad \Delta H = 2.6 \, eV/molecule \tag{2}$$

In the presence of water, CO can be easily converted into CO_2 with production of H_2, since the reaction does not require additional energy and is known as the water-gas shift reaction (WGSR):

$$CO + H_2O \rightleftarrows CO_2 + H_2, \, \Delta H^o \text{ in}$$
$$\text{forward direction} = -0.4 \, eV/molecule \tag{3}$$
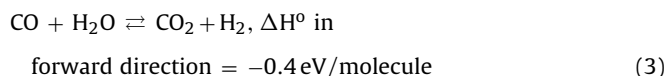
Depending on the reaction conditions, the equilibrium for WGSR can be pushed either in the forward or in the reverse direction.

By definition [10], the energy efficiency η of a dissociation process is given by:

$$\eta = \frac{\chi * \Delta H}{SEI} \tag{4}$$

where ΔH is the dissociation enthalpy of the global reaction [Eq. (1)], equal to about 2.9 eV/molecule, χ is the CO_2 conversion efficiency and SEI is the specific energy input (eV/molecule). SEI can be normally found as a ratio between the discharge power and the gas flow rate through the discharge volume.

The CO_2 conversion efficiency is calculated by comparing the GC CO_2 peak area before and after plasma processing. The conversion efficiency of CO_2 is calculated based on the following ratio:

$$\chi = \frac{\text{moles of } CO_2 \text{ converted}}{\text{moles of } CO_2 \text{ supplied}} \tag{5}$$

3.5.2. Plasma-catalytic conversion of CO_2

CO_2 conversion and energy efficiencies in the microwave discharge with and without catalysts as well as the effect of different methods of catalyst preparation are investigated. Catalysts prepared by conventional calcination or by plasma treatment were used in the plasma reactor to study the decomposition of pure CO_2. The following operating parameters were used: pure CO_2 is supplied at the flow rate of 2 slm, the mean input power is 1000 W at a pulse frequency of 1.67 kHz, which corresponds to a specific energy input of 6.95 eV/molecule, and the pressure in the discharge is set to 30 Torr (3990 Pa). In this study, we mainly focus on getting better understanding of the synergistic effect resulting from the combination of plasma and catalyst for the decomposition of pure CO_2 or CO_2 mixed with H_2O (see next section) from both physical and chemical perspectives. Fig. 8 presents the CO_2 conversion and energy efficiencies as a function of the experimental conditions (i.e. with or without catalysts). From Fig. 8, it is clear that the presence of NiO/TiO_2(Ar-P) significantly enhances the CO_2 conversion and energy efficiencies of the plasma process. The CO_2 conversion increases from 23% to 43% and the energy efficiency from 10% to 18%, compared to the plasma-only case. On the other hand, the conventional calcined catalysts (NiO/TiO_2 (Air-C) and NiO/TiO_2 (Ar-C)) affect both parameters rather insignificantly (in comparison with the plasma only-assisted CO_2 dissociation). The catalyst preparation method has a significant impact on the chemical and physical properties of the catalysts as shown above, which in turn strongly influences CO_2 conversion efficiency and its energy efficiency. It is well known that TiO_2-based catalysts are extensively studied for CO_2 photoreduction since they can be activated through the formation of electron-hole pairs with the aid of sufficient photonic
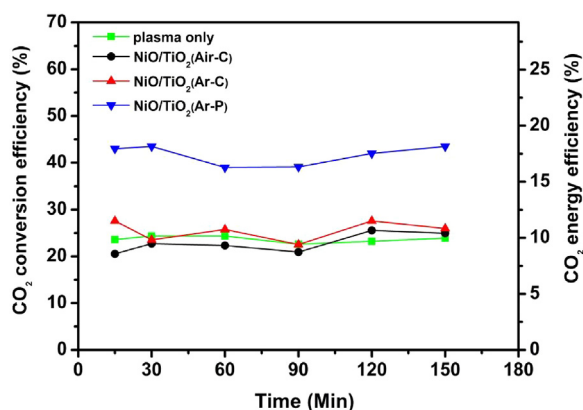
Fig. 8. Comparison of CO_2 conversion and energy efficiencies in pure plasma and the combined effects of plasma and catalysts prepared by different methods in pure CO_2.

energy. In the present investigation, CO_2 conversion and energy efficiencies in the microwave discharge with pure TiO_2 and Ar plasma treated TiO_2 (TiO_2 (Ar)) are also studied (see Fig. S3).

The photo-activation of catalyst by the ultra-violet (UV) light emitted by plasma is likely negligible in our case. Indeed, any significant differences in CO_2 conversion and its energy efficiency, compared to plasma-only assisted conversion, were observed. We therefore conclude that the observed CO_2 conversion cannot be explained by plasma activated photocatalytic conversion of CO_2. This corroborated with the recent experimental work showing that the photocatalytic properties cannot be activated by plasma irradiation because of the too low intensity of the UV radiation [19,60]. The oxygen vacancies can be the key factor explaining the catalytic activities in CO_2 decomposition. Ar plasma treatment results in a higher density of oxygen vacancies and a very good distribution of Ni oxide on the TiO_2 surface comparing with the classical calcination in air or Ar. These vacancies are stabilized by the presence of Ni^{2+} ions in the anatase lattice. The plasma pretreatment in turn allows both to create oxygen vacancies, and to incorporate the Ni into the TiO_2 lattice to stabilize these vacancies.

The pressure effect on the CO_2 decomposition was also studied, as shown in Fig. 9 in the range of 50–70 Torr (6650–9310 Pa) in the absence or presence of NiO/TiO_2(Ar-P) catalyst. Pure CO_2 is supplied at a flow rate of 6 slm, the mean input power is 1000 W at a pulse frequency of 1.67 kHz, which corresponds to a specific energy input of 2.32 eV/molecule. As shown in Fig. 9(a), our experimental data

clearly show an improvement in the CO_2 conversion with increasing the pressure, which is in good agreement with the other works related to low-pressure microwave plasma [10]. Let us mention again that pressure in our case has been controlled by changing the pumping speed rather than the gas flow. So, these pressure-dependent results should likely be associated with the different residence time of the particles, which is known to be an important parameter affecting CO_2 conversion. Indeed, the residence times estimated based on the known gas velocities in the tube (found assuming the gas temperature equal to about 1300 K (see below), and plasma active zone length of about 3 cm) are 0.7, 0.85, and 1 ms at 50, 60, and 70 Torr correspondingly. Since the residence time in the active plasma zone (where electron-vibrational (e-V) and vibrational-vibrational (V-V) energy transfer channels work efficiently) is a key parameter for efficient CO_2 dissociation, the observed elevation of the CO_2 conversion efficiency should mainly be related to the particle residence time in the plasma active zone in our case. At the same time, the changes in the CO_2 conversion induced by variations of the CO_2 vibrational excitation supposed to be rather minor, first of all due to rather narrow pressure range studied (50–70 Torr).

To verify this fact, additional visible spectroscopy analysis has been undertaken. The CO_2 emission in our case is not visible in the studied (UV–VIS) range, so the vibrational temperature has been measured based on the visible emission bands of CN (B-X, Violet band) using $CO_2 + 10\%N_2$ gas mixture. The measurements confirm that the CN vibrational excitation is rather stable in the studied pressure range, allowing us to assume that the same is also valid for CO_2 molecules (see Fig. 10), as a result of fast V–V transfer between CO_2 and CN modes. The gas temperature in the plasma area (determined by rotational temperature of the CO B $^1\Sigma^+(v'=0)$ excited state) points out on rather stable temperature behaviour in the mentioned pressure range, meaning there is no considerable vibrational-translational (V-T) energy transfer, and approving our hypothesis about the residence time to be the main factor affecting the CO_2 conversion. These results are only indicative, however, since the vibrational temperature has been measured using only three first vibrational levels of the corresponding molecular states, and it may undergo certain changes as soon as higher vibrational levels are involved.

The presence of NiO/TiO_2(Ar-P) catalyst significantly enhances the CO_2 conversion and energy efficiencies of the plasma process, as demonstrated in Fig. 9(b). The CO_2 conversion and its energy efficiency increase by a factor of 2.1 at 50 Torr. The conversion of CO_2 reaches 45% in pure CO_2 at 70 Torr, at an energy
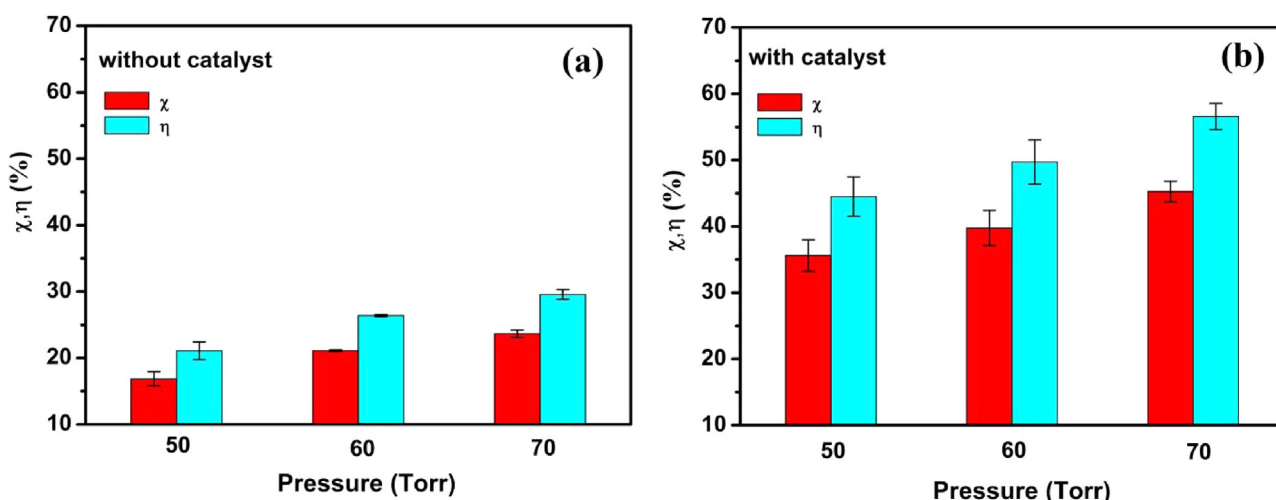

Fig. 9. Evolution of the CO_2 conversion and energy efficiencies as a function of pressure in the absence (a) or presence (b) of NiO/TiO_2(Ar-P) catalyst in pure CO_2.
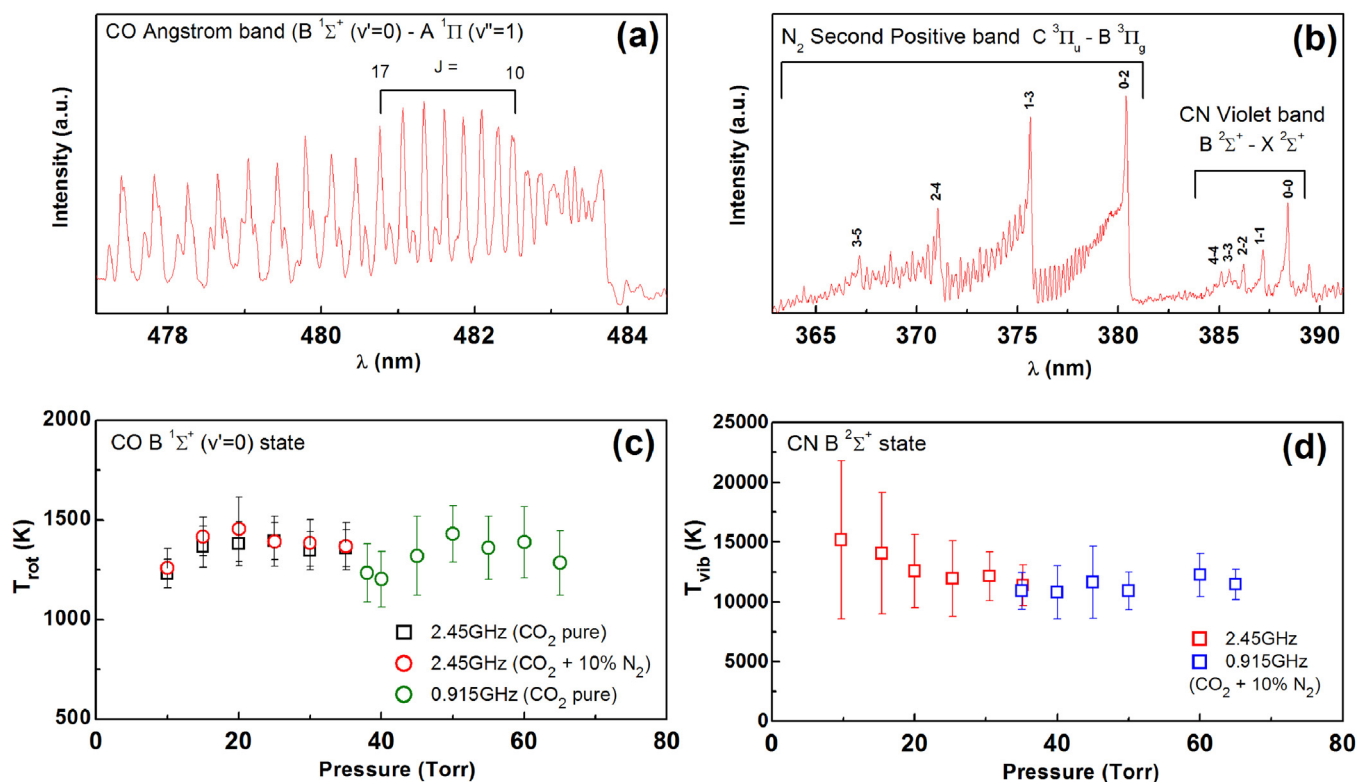
Fig. 10. The CO Angstrom (0-1) rotational band (a) and CN Violet ro-vibrational bands (b) used in this work for determination of the CO rotational temperature (c) and CN vibrational temperature (d) in the microware plasma region in the studied pressure range. The low-pressure (10–35 Torr) measurements were performed in a similar flowing gas microwave reactor working at 2.45 GHz. The total flow rate is 2 and 3 slm for 2.45 GHz and 0.915 GHz system, respectively.

efficiency of about 56%. The synergy between the plasma and Ar plasma treated NiO/TiO_2 catalyst leads to significantly improved CO_2 conversion and energy efficiencies compared to the plasma only process, regenerating the catalyst at the same time.

Fig. 11 shows a comparison of the CO_2 conversion and energy efficiencies using different types of non-thermal plasmas. A comparison between the literature results and the results obtained in this work indicates that higher conversion and energy efficiencies were achieved in the presence of $NiO/TiO_2(Ar-P)$ catalyst in our

Fig. 11. Comparison of conversion and energy efficiency for CO_2 with different types of non-thermal plasmas. □, □, ■, ■: Pure CO_2; △, ▲:CO_2-Ar mixture; ▼: CO_2-H_2O mixture; ●: CO_2-H_2O-Ar mixture. MW: Microwave; RF: Radio Frequency; GAP: Gliding arc plasmatron; MW-ss: Microwave (supersonic flow); DBD: Dielectric barrier discharge. SEI (specific energy input) is given for a reference.

case. A balance between CO_2 conversion and energy efficiency in the plasma processing of CO_2 is especially important for the development of an efficient and cost-effective plasma process for CO_2 conversion and utilization. As shown in Fig. 11, an energy efficiency of about 90% was reported by Asisov et al. when CO_2 decomposition was performed in microwave plasma in a supersonic flow [29]. However, the corresponding conversion of CO_2 was only about 10%, which is significantly lower than that obtained in this work for pure CO_2 decomposition with catalyst (45%). In this work, the combination of the microwave plasma and the $NiO/TiO_2(Ar-P)$ catalyst leads to significant enhancement in both, the conversion and energy efficiencies of the dissociation process, as well as a balance between these two parameters.

3.5.3. Plasma-catalytic conversion of CO_2/H_2O

As mentioned in the Introduction, water is a promising source of hydrogen because of its abundance and low-cost. Therefore, it is of interest to investigate plasma assisted catalytic H_2O-CO_2 conversion as an alternative system for conversion of CO_2 to value-added chemicals. Understanding the effect of the H_2O admixtures on the CO_2 plasma-assisted conversion is a first step towards understanding complex chemical plasmas in future. Plasma-catalyst assisted dissociation of CO_2 mixed with 10 vol% H_2O, 5 vol% and 10 vol% H_2 are studied. Fig. 12 presents the results on CO_2 conversion efficiency in the absence (a) or presence (b) of $NiO/TiO_2(Ar-P)$ catalyst in the different mixtures. With the plasma only experiment (Fig. 9(a)) as a reference, the CO_2 conversion efficiency increases form 23% to 30% in the CO_2-10%H_2O mixture, while it decreases to 15% in the CO_2-10% H_2 mixtures compared to the pure CO_2 case. It is well-known that the CO_2 decomposition in microwave plasmas goes predominantly via the electron impact vibrational excitation of the lowest vibrational levels, followed by the V–V energy transfer to
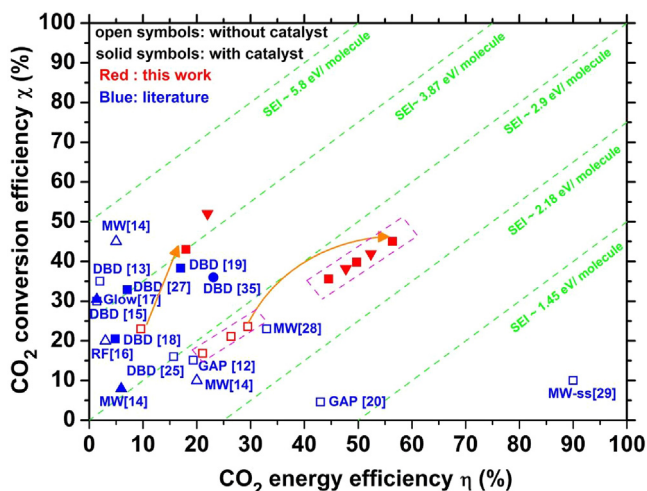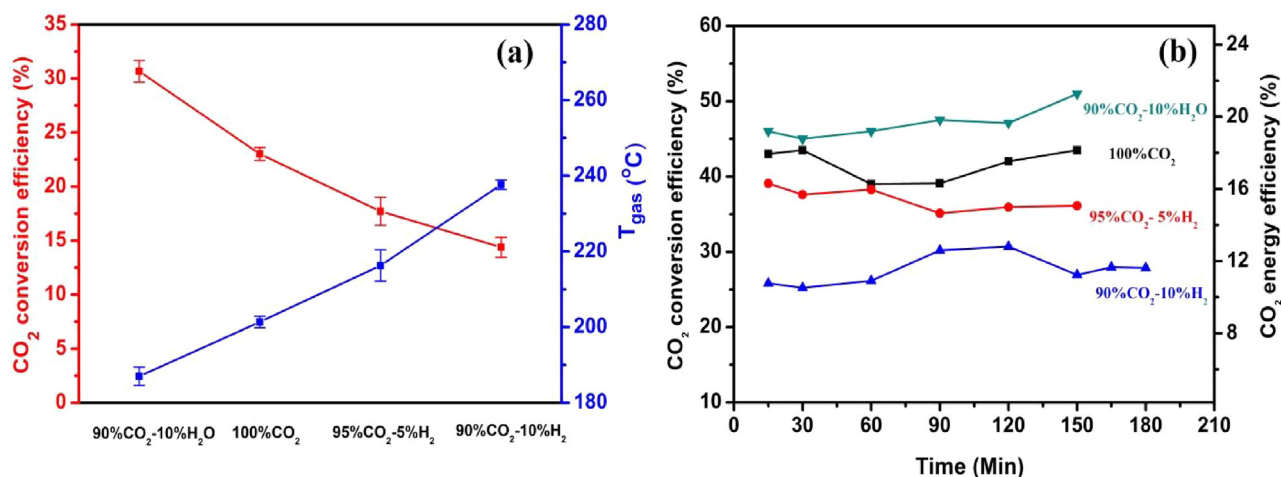
Fig. 12. Comparison of the CO_2 conversion efficiency in different gas mixtures (CO_2 pure, with H_2O and with H_2) and in the absence (a) or presence (b) of NiO/TiO_2(Ar-P) catalyst. Gas temperature (T_{gas}) is also measured in the catalyst chamber (post-discharge) for different gas mixture. Flow rate = 2 slm; Pressure = 30 Torr; SEI = 6.95 eV/molecule. Pulse frequency = 1.67KHz.

the higher vibrational states of CO_2 which are efficient for the CO_2 decomposition [10]:

$$CO_2 + e^- \rightarrow CO_2{}^{vib} + e^- \rightarrow CO + O + e^- \qquad (6)$$
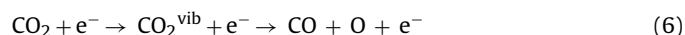
where $CO_2{}^{vib}$ is the vibrational excited state. Since the energy barriers for exciting CO_2 are lower than the energy barriers for direct dissociation, the stepwise vibrational excitation process is common in CO_2 plasma [10]. The different CO_2 conversion efficiencies maybe linked to the gas temperature in the different gas mixtures measured in the post discharge and given in Fig. 12(a). It was reported that the presence of H_2 significantly decreases the electron temperature of the gas mixture [61], which should impair the vibrational excitation of CO_2. The higher gas temperature gives rises to more vibrational-translational relaxation collisions of the CO_2 vibrational levels, which is the most important loss mechanism for the CO_2 vibrational population [62]. This will considerably decrease CO_2 conversion efficiency as observed in Fig. 11(a) with increasing of H_2 content. This explains the lower conversion efficiency in CO_2/H_2 mixtures.

The study of CO_2 conversion efficiency in different gas mixtures in the presence of NiO/TiO_2 (Ar-P) leads to similar trends, as shown in Fig. 12(b). Moreover, it was found that the CO_2 con-

version efficiency was also enhanced independently of the mixture when NiO/TiO_2 (Ar-P) is used. A synergism between the catalyst and plasma is clearly demonstrated in this case. The CO_2 conversion and energy efficiencies in $90\%CO_2$-$10\%H_2O$ increase from 30% to 52% and 12.5% to 22%, respectively, when the activated catalyst is combined with the plasma. Evolution of the CO_2 conversion and energy efficiencies as a function of pressure was also studied in 50 Torr and 60 Torr in the absence or presence of NiO/TiO_2(Ar-P) catalyst in CO_2/H_2O mixture. The measurement could not be performed for CO_2/H_2O mixture at 70 Torr due to the setup limitations. As demonstrated in Fig. 13, the increase of pressure leads to an improvement of the CO_2 conversion process in CO_2-10% H_2O mixture with and without catalyst. Similar trends have been observed in the pure CO_2 case in the Section 3.5.2.

As mentioned above, the main gas phase dissociation mechanism in the microwave plasma is the stepwise vibrational excitation of CO_2 molecule. At the catalyst surface with oxygen vacancies this mechanism is different being represented by dissociative electron attachment. The synergy between the plasma and Ar plasma treated NiO/TiO_2 catalyst leads to significantly improved CO_2 conversion and energy efficiencies compared to the plasma only process. The constant efficiencies over time prove that the cat-
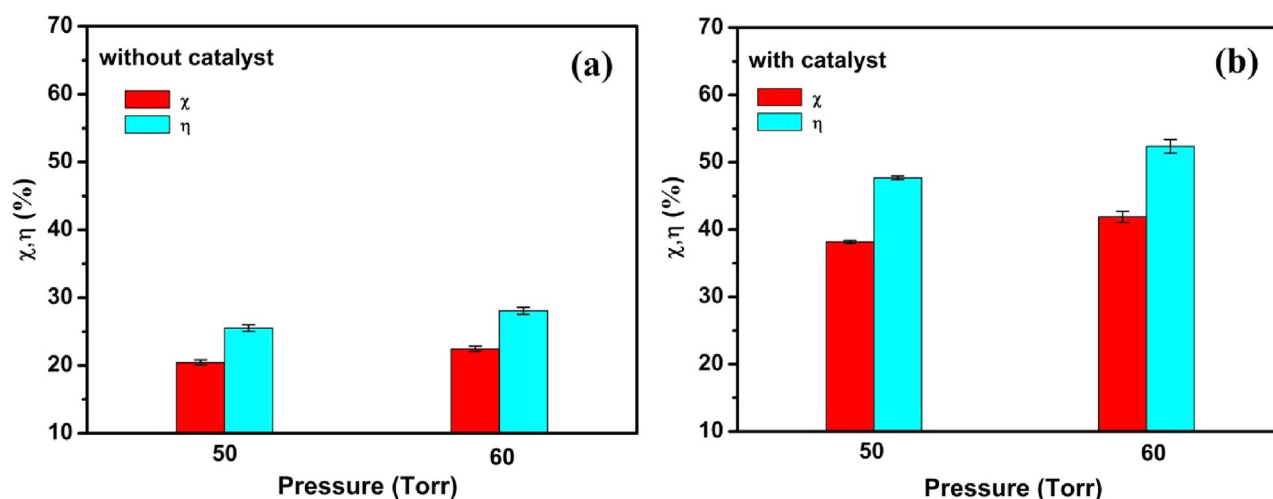

Fig. 13. Evolution of the CO_2 conversion and energy efficiencies as a function of pressure in the absence (a) or presence (b) of NiO/TiO_2(Ar-P) catalyst in CO_2-10%H_2O mixture. Flow rate = 6 slm; SEI = 2.32 eV/molecule. Pulse frequency = 1.67KHz.

alyst is regenerated at the same time. According to the mechanism reported for photocatalytic CO_2 reduction with H_2O, Hydrogen radicals would induced the direct hydrogenation of CO_2 and reduce CO_2 to CO on a catalyst surface via the following reaction [36,63,64]:

$$H + CO_2 \rightarrow OH + CO \tag{7}$$

Arita et al. found that CO_2 can be decomposed to form CO by H radicals or H_2 in a low-pressure CO_2/H_2 discharge and the very low amount of H_2 was necessary for proceeding this reaction with CO_2 [65]. This reaction may also contribute to the improved CO_2 conversion efficiency in presence of NiO/TiO_2 (Ar-P) for CO_2/H_2O and CO_2/H_2 mixtures.

The achieved values of the CO_2 conversion and energy efficiency in CO_2/H_2O mixture in this section are also added in Fig. 11 for a comparison. Mahammadunnisa et al. reported a maximum conversion of 36% with an energy efficiency of 23% in the case of $Ni/\gamma-Al_2O_3$ catalyst at a flow rate of 20 ml min^{-1} [35]. In that study, only 10 vol% CO_2 is mixed with argon and 2.3 vol% water vapor. However, a high conversion at a very low flow rate and long residence time is not attractive for industrial applications. In this work, the conversion of CO_2 reaches 42% in the presence of Ar plasma treated catalyst in CO_2/H_2O mixture at a flow rate of 61 min^{-1}, which corresponds to the energy efficiency of about 52%. The comparison shows the efficiency of microwave discharges combined with plasma treated catalyst for improving CO_2 conversion.

An increasing interest has been shown to the fabrication of oxygen-deficient surfaces recently, which is an important strategy for improving the photocatalytic CO_2 dissociation [46]. Both theoretical and experimental studies consistently showed that the CO_2 adsorption, activation and dissociation were strongly influenced by the defect disorders in TiO_2 [67]. The defect disorders such as oxygen vacancy have been considered as the active site for the CO_2 activation. The electron trapped into an oxygen vacancy can be spontaneously transferred to CO_2 bring about the formation of CO_2^- anion. CO_2^- anion may decompose into CO through the occupation of one oxygen atom into the oxygen vacancy site. This dissociation electron attachment process for CO_2 occurs more easily for the adsorbed CO_2 at the oxygen vacancy than for CO_2 in the gas phase since the threshold energy of 1.4 eV is much lower compared to the threshold energy of 5–10 eV in the gas phase [66]. Recently density functional theory calculations studies [68] show that oxygen vacancies play a significant role in the dissociation of CO_2 on the anatase surface. The introduction of oxygen vacancy defects gives rise to new highly stable adsorption configurations with a stronger activation of the C—O bonds. The electrons supplied by the plasma can enhance the dissociative attachment of CO_2 on the oxygen-deficient catalyst surface [8]. Fig. 5 and Fig. 7 indicate that the plasma treatment of the catalyst NiO/TiO_2(Ar-P) can result in a higher density of oxygen vacancies compared to the conventional calcined one (NiO/TiO_2 (Air-C) and NiO/TiO_2 (Ar-C)). We suggest that the following processes can be distinguished on the catalyst surface in the plasma-catalytic CO_2/H_2O conversion (Fig. 14). CO_2 could be reduced to CO via reaction with H radical or direct dissociation by healing the oxygen vacancy sites [63–65]. The active species OH and adsorbed oxygen atom react with each other to form atomic hydrogen and O_2, resulting in the regeneration of oxygen vacancy. The oxygen vacancy can also be regenerated via the recombination on the surface of a bridging oxygen atom with a gaseous oxygen atom [69–71]. The plasma supplies energy to the catalyst surface and thus additionally enhances the recombination process. The regeneration of the oxygen vacancies can be confirmed by our experimental results shown in Fig. 8 and Fig. 12(b). The CO_2 conversion and energy efficiencies remain more or less constant over time at least for 150 min of continuous operation (as verified additinally). Hence, a synergistic effect between the plasma and the NiO/TiO_2(Ar-P) catalyst leads to significantly improved CO_2
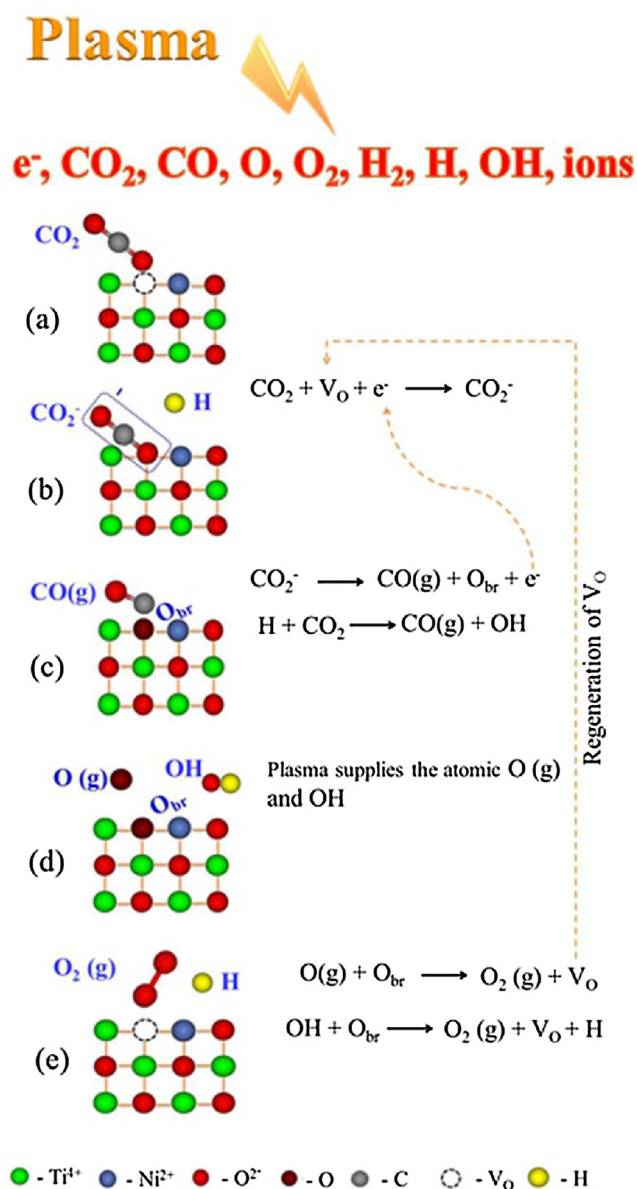

Fig. 14. Possible reaction mechanism of plasma–catalytic conversion of CO_2 mixed with H_2O on the surface of catalyst. (a) Adsorption, (b)+(c) DEA process, (d)+(e) Vo regeneration via formation of O_2 on the surface and its desorption.

conversion and energy efficiencies, which can be attributed to the dominant surface reactions driven by the plasma.

4. Conclusions

In this study, the plasma-catalytic conversion of CO_2 in the presence or absence of H_2O vapor has been investigated in a low-pressure microwave plasma system combined with TiO_2-supported NiO catalysts. It was demonstrated that the catalyst preparation method affects significantly the chemical and physical properties of the considered catalysts, which in turn strongly influence the CO_2 conversion and the energy efficiencies of the process. More precisely, the utilization of the catalyst prepared by the Ar plasma irradiation results in a nearly twofold increase of the CO_2 conversion and energy efficiencies, while the conventional calcined (whether in air or in Ar) catalysts show an insignificant improvement in CO_2 conversion comparing to the plasma-only CO_2 dissociation process.

The maximum values of CO_2 conversion and energy efficiencies attained in this work are 45% and 56%, respectively, which corresponds to the pure CO_2 case and 70 Torr of the gas pressure in the presence of Ar plasma–treated catalyst. On the other hand, in the case of CO_2/H_2O mixture, the CO_2 conversion efficiency reaches 42% (energy efficiency is 52%) at 60 Torr.

Comparison with the literature results approves effectiveness of the microwave discharges combined with plasma-treated catalyst for improvements of CO_2 conversion and its energy efficiencies. We suggest that the oxygen vacancies stabilized by the presence of Ni^{2+} ions in the TiO_2 anatase lattice may be a key factor for high catalytic activities during the CO_2 conversion process in microwave plasmas. The plasma pretreatment process allows both creation of the oxygen vacancies, and Ni atoms incorporation into the TiO_2 lattice, thus resulting in stabilization of these vacancies. On the other hand, dissociative electron attachment of CO_2 at the catalyst surface enhanced by the oxygen vacancies and plasma electrons as well as the water-based metastable species can explain the increase in the CO_2 conversion and its energy efficiency.

Acknowledgments

Appendix A. Supplementary data

Supplementary data associated with this article can be found, in the online version, at http://dx.doi.org/10.1016/j.apcatb.2017.05.032.

References

[1] C. Liu, G. Xu, T. Wang, Fuel Process. Technol. 58 (1999) 119–134.
[2] H.L. Chen, H.M. Lee, S.H. Chen, Y. Chao, M.B. Chang, Appl. Catal. B 85 (2008) 1–9.
[3] J. Van Durme, J. Dewulf, C. Leys, H. Van Langenhove, Appl Catal B 78 (2008) 324–333.
[4] A.M. Ghorbanzadeh, R. Lotfalipour, S. Rezaei, Int. J. Hydrogen Energy. 34 (2009) 293–298.
[5] H. Long, S. Shang, X. Tao, Y. Yin, X. Dai, Int. J. Hydrogen Energy 33 (2008) 5510–5515.
[6] X. Tu, J.C. Whitehead, Appl. Catal. B 125 (2012) 439–448.
[7] H.J. Gallon, X. Tu, M.V. Twigg, J.C. Whitehead, Appl. Catal. B 106 (2011) 616–620.
[8] G. Chen, V. Georgieva, T. Godfroid, R. Snyders, M.-P. Delplancke-Ogletree, Appl. Catal. B: Environ. 190 (2016) 115–124.
[9] X. Tu, H.J. Gallon, J.C. Whitehead, Catal. Today 211 (2013) 120–125.
[10] A. Fridman, Plasma Chemistry, Cambridge University Press, 2008.
[11] G. Zheng, J. Jiang, Y. Wu, R. Zhang, H. Hou, Plasma Chem. Plasma Process. 23 (2003) 59–68.
[12] A. Indarto, D.R. Yang, J.W. Choi, H. Lee, H.K. Song, J. Hazard. Mater. 146 (2007) 309–315.
[13] R. Aerts, W. Somers, A. Bogaerts, 2015, ChemSusChem 8 (2015) 702–716.
[14] L.F. Spencer, A.D. Gallimore, Plasma Sources Sci. Techenol. 22 (2013) 015019.
[15] S. Paulussen, B. Verheyde, T. Xin, C.D. Bie, T. Martens, D. Petrovic, A. Bogaerts, B. Sels, Plasma Sources Sci. Technol. 19 (2010) 034015.
[16] L.F. Spencer, A.D. Gallimore, Plasma Chem. Plasma Process. 31 (2011) 79–89.
[17] S.L. Brock, M. Marquez, S.L. Suib, Y. Hayashi, H. Matsumoto, J. Catal. 180 (1998) 225–233.
[18] Q. Yu, M. Kong, T. Liu, J. Fei, X. Zheng, 2012, Plasma Chem. Plasma Process. 32 (2012) 153–163.
[19] D. Mei, X. Zhu, C. Wu, B. Ashford, P.T. Williams, X. Tu, Appl. Catal. B. 182 (2016) 525–532.
[20] T. Nunnally, K. Gutsol, A. Rabinovich, A. Fridman, A. Gutsol, A. Kemoun, J. Phys. D: Appl. Phys. 44 (2011), 274009 (7pp).
[21] G. Chen, N. Britun, T. Godfroid, R. Snyders, M.-P. Delplancke-Ogletree, J. Phys. D: Appl. Phys. 50 (2017) 084001.
[22] R. Snoeckx, S. Heijkers, K. Van Wesenbeeck, S. Lenaerts, A. Bogaerts, Energ. Environ. Sci. 9 (2016) 999–1011.
[23] S.R. Sun, H.X. Wang, D.H. Mei, X. Tu, A. Bogaerts, J. CO2 Util. 17 (2017) 220–234.
[24] T. Silva, N. Britun, T. Godfroid, R. Snyders, Plasma Process. Polym. (2016), http://dx.doi.org/10.1002/ppap.201600103.
[25] A. Ozkan, T. Dufour, A. Bogaerts, F. Reniers, Plasma Sources Sci. Technol. 25 (4) (2016) 045016.
[26] B. Ashford, X. Tu, Curr. Opin. Green Sustainable Chem. 3 (2017) 45–49.
[27] X.F. Duan, Z.Y. Hu, Y.P. Li, B.W. Wang, AIChE J. 61 (2015) 898–903.
[28] T. Silva, N. Britun, T. Godfroid, R. Snyders, Study of CO2 Decomposition in Microwave Discharges by Optical Diagnostic Methods. Plasma science and technology – progress in physical states and chemical reactions, InTech (2016), http://dx.doi.org/10.5772/61854.2016.
[29] R.I. Asisov, V.K. Givotov, E.G. Krasheninnikov, B.V. Potapkin, V.D. Rusanov, A. Fridman, Sov. Phys. Dokl. 271 (1983) 94.
[30] G.J. van Rooij, D.C.M. van den Bekerom, N. den Harder, T. Minea, G. Berden, W.A. Bongers, R. Engeln, M.F. Graswinckel, E. Zoethout, M.C.M. van de Sanden, Faraday Discuss. 183 (2015) 233.
[31] C. De Bie, J. Dijk, A. Bogaerts, J. Phys. Chem. C 120 (2016) 25210–25224.
[32] E. Jwa, S.B. Lee, H.W. Lee, Y.S. Mok, Fuel Process. Technol. 108 (2013) 89–93.
[33] Y. Zeng, X. Tu, J. Phys. D: Appl. Phys. 50 (2017) 184004.
[34] G. Chen, T. Silva, V. Georgieva, T. Godfroid, N. Britun, R. Snyders, M.-P. Delplancke-Ogletree, Int. J. Hydrogen Energy 40 (2015) 3789–3796.
[35] S. Mahammadunnisa, L. Reddy, D. Ray, C. Subrahmanyam, J.C. Whitehead, Int. J. Greenh. Gas Con. 16 (2013) 361–363.
[36] R. Snoeckx, A. Ozkan, F. Reniers, A. Bogaerts, ChemSusChem 10 (2017) 409–424.
[37] M.B. Kizling, S.G. Järäs, M. Appl. Catal. A 147 (1996) 1–21.
[38] C. Liu, G.P. Vissokovb, B.W.L. Jang, Catal. Today 72 (2002) 173–184.
[39] C. Liu, J. Zou, K. Yu, D. Cheng, Y. Han, J. Zhan, C. Ratanatawanate, B.W.L. Jang, Pure. Appl. Chem. 78 (2006) 1227–1238.
[40] W.C. Chung, M.B. Chang, Renew. Sustain. Energy Rev. 62 (2016) 13–31.
[41] T. Godfroid, J.P. Dauchot, M. Hecq, Surf. Coat. Technol. 200 (2005) 649.
[42] X. Zhu, P. Huo, Y. Zhang, D. Cheng, C. Liu, Appl. Catal. B: Environ. 81 (2008) 132–140.
[43] J. Zhang, M. Li, Z. Feng, J. Chen, C. Li, J. Phys. Chem. B 110 (2006) 927–935.
[44] B. Choudhury, A. Choudhhury, Mater. Chem. Phys. 132 (2012) 1112–1118.
[45] F. Tian, Y. Zhang, J. Zhang, C. Pan, J. Phys. Chem. C 112 (2012) 7515–7519.
[46] H.Y. Lin, Y.Y. Chou, C.L. Cheng, Y.F. Chen, Opt. Express 15 (2007) 13832–13837.
[47] L. Liu, H. Zhao, J.M. Andino, Y. Li, ACS Catal. 2 (2012) 1817–1828.
[48] C. Chagas, E.F. de Souza, R.L. Manfro, S.M. Landi, M.M.V.M. Souza, M. Schmal, Appl. Catal. B: Environ. 182 (2016) 257–265.
[49] S. Chen, S. Zhang, W. Liu, W. Zhao, J. Hazard. Mater. 155 (2008) 320–326.
[50] A.V. Naumkin, S.W. Kraut-Vass, C.J. Powell, NIST X-Ray Photoelectron Spectroscopy Database, 20, 2012 (Version 4.1).
[51] Y. Tong, L. Chen, S. Ning, N. Tong, Z. Zhang, H. Lin, F. Li, X. Wang, Appl. Catal. B: Environ. 203 (2017) 725–730.
[52] G. Chen, Q. Li, Y. Wei, W. Fang, Y. Yang Chin, J. Catal. 34 (2013) 322–329.
[53] B. Bharti, S. Kumar, H.N. Lee, R. Kumar, Sci. Rep. 6 (2016) 32355.
[54] R. Sanjinés, H. Tang, H. Berger, F. Gozzo, G. Margaritondo, F. Lévy, J. Appl. Phys. 75 (1994) 2945–2951.
[55] L. Lin, K. Wang, K. Yang, X. Chen, X. Fu, W. Dai, Appl. Catal. B: Environ. 204 (2017) 440–455.
[56] J. Tyczkowski, Cold plasma produced catalytic materials, plasma science and technology – progress in physical states and chemical reactions, InTech (2016), http://dx.doi.org/10.5772/61832.
[57] J. van Dijk, K.S.C. Peerenboom, M. Jimenez-Diaz, D.B. Mihailova, J.J.A.M. van der Mullen, J. Phys. D: Appl. Phys. 42 (2009) 194012.
[58] The Plasimo code website: http://plasimo.phys.tue.nl/.
[59] V. Georgieva, A. Berthelot, T. Silva, St. Kolev, W. Graef, N. Britun, G. Chen, J. van der Mullen, T. Godfroid, D. Mihailova, J. van Dijk, R. Snyders, A. Bogaerts, M.-P. Delplancke-Ogletree, Plasma Processes Polym. 14 (2017), 1600185.
[60] H.H. Kim, Y. Teramoto, N. Negishi, A. Ogata, Catal. Today 256 (2015) 13–22.
[61] I. Dobrea, S. Popa, 31 st ICPIG, July 14–19, Granada Spain (2013).
[62] T. Kozák, A. Bogaerts, Plasma Sources Sci. Technol. 23 (2014) 045004.
[63] M. Tahir, B. Tahir, N.A.S. Amin, A. Muhammad, Energy Convers. Manage. 119 (2016) 368–378.
[64] Y. Li, W. Wang, Z. Zhan, M. Woo, C.Y. Wu, P. Biswas Appl, Catal. B 100 (2010) 386–392.
[65] K. Arita, S. Iizuka, BJAST 15 (2016) 1–8.
[66] J. Lee, D.C. Sorescu, X. Deng, J. Am. Chem. Soc. 133 (2011) 10066–10069.
[67] L. Liu, Y. Li Aerosol, Air. Qual. Res 14 (2014) 453–469.
[68] S. Huygh, A. Bogaerts, E.C. Neyts, J. Phys. Chem. C 120 (2016) 21659–21669.
[69] P.G. Dickens, M.B. Sutcliffe, Trans. Faraday Soc. 60 (1964) 1272–1285.
[70] P.J. Crane, P.G. Dickens, R.E. Thomas, Trans. Faraday Soc. 63 (1967) 693–700.
[71] V.L. Kovalev, A.A. Krupnov, M.Yu. Pogosbekyan, L.P. Sukhanov, Acta Astronaut. 68 (2011) 686–690.